NASA TECHNICAL MEMORANDUM

NASA TM X-72754

CRACK GROWTH IN Ti-8Al-1Mo-1V WITH REAL-TIME AND ACCELERATED FLIGHT-BY-FLIGHT LOADING

BY L. A. IMIG

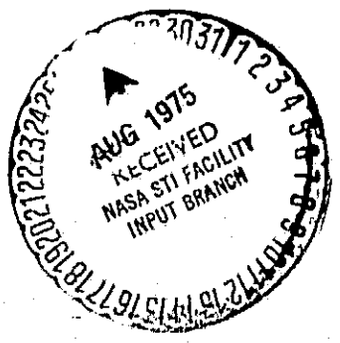

NATIONAL AERONAUTICS AND SPACE ADMINISTRATION
LANGLEY RESEARCH CENTER, HAMPTON, VIRGINIA 23665

NASA TECHNICAL MEMORANDUM

NASA TM X-72754

NASA TM X-72754

(NASA-TM-X-72754) CRACK GROWTH IN Ti-8Al-1Mo-1V WITH REAL-TIME AND ACCELERATED FLIGHT BY FLIGHT LOADING (NASA) 35 p HC $3.75 CSCL 01C

N75-29092

Unclas
G3/05 32388

CRACK GROWTH IN Ti-8Al-1Mo-1V WITH REAL-TIME AND ACCELERATED FLIGHT-BY-FLIGHT LOADING

BY L. A. IMIG

NATIONAL AERONAUTICS AND SPACE ADMINISTRATION
LANGLEY RESEARCH CENTER, HAMPTON, VIRGINIA 23665

1. Report No.	2. Government Accession No.	3. Recipient's Catalog No.
TM X-72754		

4. Title and Subtitle	5. Report Date
CRACK-GROWTH IN Ti-8Al-1Mo-1V WITH REAL-TIME AND ACCELERATED FLIGHT-BY-FLIGHT LOADING	July 30, 1975
	6. Performing Organization Code

7. Author(s)	8. Performing Organization Report No.
L. A. Imig	
	10. Work Unit No.

9. Performing Organization Name and Address	11. Contract or Grant No.
NASA Langley Research Center Hampton, VA 23665	
	13. Type of Report and Period Covered
12. Sponsoring Agency Name and Address	Technical Memorandum
National Aeronautics and Space Administration Washington, D.C. 20546	14. Sponsoring Agency Code 505-02-31-01

15. Supplementary Notes

16. Abstract

Crack growth in Ti-8Al-1Mo-1V was measured and calculated for real-time and accelerated simulations of supersonic airplane loading and heating. Crack-growth rates calculated on the assumption that an entire flight could be represented by a single cycle predicted the experimental rates poorly. Calculated crack-growth rates were slower than the experimental rates for all tests with flight-by-flight loading. For room-temperature accelerated tests, the calculated rates agreed well with the experimental rates; but the calculations became progressively less accurate for progressively more complex test conditions (tests that included elevated temperature). Calculations of crack growth using the crack-closure concept can probably be improved through study of crack-opening stresses using finite-element models that account for variable-amplitude loading, residual stresses, and temperature effects. The calculations of crack growth could also be improved through detailed studies of material properties and interactions among stress, temperature, and time as appropriate for the real-time operating conditions of a supersonic transport airplane.

Little quantitative information about crack growth was available from scanning-electron fractographs because little fatigue detail was present.

17. Key Words (Suggested by Author(s)) (STAR category underlined)	18. Distribution Statement
Fatigue (materials), stress cycle, elevated temperature, supersonic transports, titanium alloy, flight simulation, axial stress, accelerated tests, crack initiation, crack propagation, scanning-electron microscopy.	Unclassified - Unlimited

19. Security Classif. (of this report)	20. Security Classif. (of this page)	21. No. of Pages	22. Price*
UNCLASSIFIED	UNCLASSIFIED	35	$3.75

*Available from { The National Technical Information Service, Springfield, Virginia 22151
STIF/NASA Scientific and Technical Information Facility, P.O. Box 33, College Park, MD 20740

1. Report No.	2. Government Accession No.	3. Recipient's Catalog No.
TM X-72754		

4. Title and Subtitle	5. Report Date
CRACK-GROWTH IN Ti-8Al-1Mo-1V WITH REAL-TIME AND ACCELERATED FLIGHT-BY-FLIGHT LOADING	July 30, 1975
	6. Performing Organization Code

7. Author(s)	8. Performing Organization Report No.
L. A. Imig	
	10. Work Unit No.

9. Performing Organization Name and Address	11. Contract or Grant No.
NASA Langley Research Center Hampton, VA 23665	

12. Sponsoring Agency Name and Address	13. Type of Report and Period Covered
National Aeronautics and Space Administration Washington, D.C. 20546	Technical Memorandum
	14. Sponsoring Agency Code 505-02-31-01

15. Supplementary Notes

16. Abstract

Crack growth in Ti-8Al-1Mo-1V was measured and calculated for real-time and accelerated simulations of supersonic airplane loading and heating. Crack-growth rates calculated on the assumption that an entire flight could be represented by a single cycle predicted the experimental rates poorly. Calculated crack-growth rates were slower than the experimental rates for all tests with flight-by-flight loading. For room-temperature accelerated tests, the calculated rates agreed well with the experimental rates; but the calculations became progressively less accurate for progressively more complex test conditions (tests that included elevated temperature). Calculations of crack growth using the crack-closure concept can probably be improved through study of crack-opening stresses using finite-element models that account for variable-amplitude loading, residual stresses, and temperature effects. The calculations of crack growth could also be improved through detailed studies of material properties and interactions among stress, temperature, and time as appropriate for the real-time operating conditions of a supersonic transport airplane.

Little quantitative information about crack growth was available from scanning-electron fractographs because little fatigue detail was present.

17. Key Words (Suggested by Author(s)) (STAR category underlined)	18. Distribution Statement
Fatigue (materials), stress cycle, elevated temperature, supersonic transports, titanium alloy, flight simulation, axial stress, accelerated tests, crack initiation, crack propagation, scanning-electron microscopy.	Unclassified - Unlimited

19. Security Classif. (of this report)	20. Security Classif. (of this page)	21. No. of Pages	22. Price*
UNCLASSIFIED	UNCLASSIFIED	35	$3.75

*Available from { The National Technical Information Service, Springfield, Virginia 22151
STIF/NASA Scientific and Technical Information Facility, P.O. Box 33, College Park, MD 20740

CRACK GROWTH IN Ti-8Al-1Mo-1V WITH REAL-TIME AND ACCELERATED FLIGHT-BY-FLIGHT LOADING

L. A. Imig

NASA Langley Research Center
Hampton, Virginia 23665, U.S.A.

Presented at the ASTM 78th Annual Meeting
Symposium on Fatigue Crack Growth Under Spectrum Loads

Montreal, Canada
June 23-24, 1975

CRACK GROWTH IN Ti-8Al-1Mo-1V WITH REAL-TIME AND ACCELERATED FLIGHT-BY-FLIGHT LOADING

L. A. Imig
NASA Langley Research Center
Hampton, Virginia 23665, U.S.A.

ABSTRACT

Crack growth in Ti-8Al-1Mo-1V was measured and calculated for real-time and accelerated simulations of supersonic airplane loading and heating. Crack-growth rates calculated on the assumption that an entire flight could be represented by a single cycle predicted the experimental rates poorly. Calculated crack-growth rates were slower than the experimental rates for all tests with flight-by-flight loading. For room-temperature accelerated tests, the calculated rates agreed well with the experimental rates; but the calculations became progressively less accurate for progressively more complex test conditions (tests that included elevated temperature). Calculations of crack growth using the crack-closure concept can probably be improved through study of crack-opening stresses using finite-element models that account for variable-amplitude loading, residual stresses, and temperature effects. The calculation of crack growth could also be improved through detailed studies of material properties and interactions among stress, temperature, and time as appropriate for the real-time operating conditions of a supersonic transport airplane.

Little quantitative information about crack growth was available from scanning-electron fractographs because little fatigue detail was present.

KEY WORDS: Fatigue (materials), stress cycle, elevated temperature, supersonic transports, titanium alloy, flight simulation, axial stress, accelerated tests, crack initiation, crack propagation, scanning electron microscopy.

L-9909

INTRODUCTION

Practical aspects of fatigue-crack growth are a concern shared by both researchers and designers. Crack growth related to airplane materials and structures has been studied predominantly for subsonic airplane conditions, as in References 1 and 2, for recent examples; but crack growth for materials and conditions representing supersonic flight also requires study to stay abreast of advancing flight capabilities. (Such advancement has led to the Anglo-French Concorde and the Russian Tu-144 supersonic airplanes.) The objectives of the present paper were to determine the effects on crack growth of the real-time and temperature environment of simulated Mach 3 flight, and to assess the applicability of the crack-closure and linear summation methods to crack-growth calculations for these flight-simulation tests.

SYMBOLS

a	One-half of overall crack length including notch, m
a_ℓ	Distance from center of specimen to tip of long crack, m
a_s	Distance from center of specimen to tip of short crack, m
Δa	Change in crack length during an interval of crack growth, m
b	Half length of center notch, m
c	Half height of center notch, m
C	Constant in the relation between crack-growth rate and ΔK_{eff}, when rate is in mm/flight and ΔK_{eff} is in MPa $\sqrt{m}$
$\bar{C}$	Constant in the relation between crack-growth rate and ΔK, when rate is in mm/flight and ΔK is in MPa $\sqrt{m}$
e	Eccentricity of long and short cracks $(a_\ell - a_s)/2$, m

ΔK	Range of stress intensity, MPa $\sqrt{m}$
ΔK_{eff}	Range of effective stress intensity, MPa $\sqrt{m}$
L	Factors from Reference 9
n	Exponent in crack-growth relation
ΔN	Interval of crack growth, flights
R	Minimum stress divided by maximum stress
S	Stress, Pa
ΔS	Range of stress, Pa
U	Factor defining effective stress range
W	Width of specimen, m

EXPERIMENTAL CONSIDERATIONS

Materials and Specimens

The crack-growth tests for this investigation were conducted on duplex-annealed Ti-8Al-1Mo-1V, titanium alloy sheet which was 1.27 mm thick. The tensile properties of the sheet agreed closely with those from Reference 3 for this alloy.

The fatigue specimens made from the sheet titanium alloy are shown in Figure 1. The central notch produced a stress-concentration factor of 4.1. Parallel reference lines spaced at 1.27 mm were photographically placed on accelerated test specimens for use in recording crack lengths.

Stress Sequences

The present fatigue tests used programed variable-amplitude stress sequences ("flights") representing the stresses expected in the lower wing skin of a commercial supersonic transport during its operation. The flights were derived in Reference 4 considering atmospheric turbulence, flight maneuvers, and landing as sources of wing load. Reference 4 describes the

formulation of variable-amplitude flights whose largest amplitude was calculated to occur, on the average, once per flight, once in five flights, once in a hundred flights, and so forth. The stresses within the flights were determined separately for the climb, cruise, and descent segments of flight as shown in Figure 2 for the flight whose largest amplitude occurred once per flight. The design mean stress referred to in Figure 2 represents the stress in a lower wing skin during level unaccelerated flight at maximum airplane mass.

The flights developed in Reference 4 are called type-A flights. They were simplified to produce an additional sequence of variable-amplitude flights called type-G flights, see Figure 2(b). Type-G flights consisted of a single cycle having the same maximum and minimum stresses as each of the flights from which they were taken.

Fatigue Tests

Two kinds of fatigue tests, called "real-time" and "accelerated," were conducted to compare crack growth for the realistic time and temperature environment of a supersonic airplane relative to the crack growth from fatigue tests which neglect time and temperature effects. Both the real-time and accelerated tests employed identical sequences of stress amplitudes within the flights. In accelerated type-A tests, both the stress sequence within each flight and the order in which the flights were applied were scheduled automatically by a computer; the flights of Figure 2(a) were applied at a rate of about 2 seconds each, and the test was conducted either at room temperature or constant elevated temperature. In real-time tests, the flights were inscribed on charts for a chart-following device; each flight,

Figure 2(c), lasted about 96 minutes, and included a 90-minute-long elevated temperature cycle.

All fatigue tests employed hydraulically actuated, closed-loop, servo-controlled fatigue testing machines (Ref. 5) which operated 24 hours a day. The specimens were loaded axially. Stresses for accelerated tests were based on the initial net area at the test section of each single notch specimen; for real-time tests, stresses were based on the average net area of each six-notch specimen. In a given six-notch specimen, the individual net areas of the notches were within 1 percent of the average area.

Crack-Growth Recording--Specimens for real-time tests were visually inspected approximately monthly for crack initiation. After cracks were discovered, their growth was logged weekly by an optical inspection with a 10-power microscope. In accelerated tests, crack growth was recorded by a 70-mm camera which simultaneously photographed the specimen and a flight counter. A special command included in the sequence of flight loads activated the camera and advanced the film by one frame. The image on the film was approximately full size and crack lengths were determined from the spacing of the reference lines on the specimen.

Test Conditions--The type-A flights were used in tests with design mean stresses of 172, 207, and 241 MPa, as shown in Table 1. One accelerated test was conducted at room temperature (300 K) and one at 560 K for each design stress. In real-time tests, the temperature was cycled from 300 K to 560 K in each flight (see Fig. 2(c)).

Type-G flights were used on one set of room-temperature accelerated tests (see Table 1). Tests with type-G stress sequences were conducted as a potential aid in analyzing the crack growth in tests with type-A stress sequences.

CRACK-GROWTH ANALYSIS

Crack growth from both constant-amplitude tests and the present variable-amplitude tests was analyzed in terms of growth rate and stress intensity. The analyses are discussed in the two following sections.

Constant-Amplitude Tests

The crack-growth data for constant-amplitude tests of Ti-8Al-1Mo-1V (Ref. 6) were analyzed using the crack-closure concept of Reference 7 to define an effective stress-intensity factor. According to that concept, the crack is closed during part of each load cycle and therefore cannot grow during that time; thus, the applied stress range ΔS is reduced to an effective stress range of $U\Delta S$. The factor U was determined (Ref. 7) for crack growth at positive R values in an aluminum alloy. For expediency, the same factor U was used in this paper to analyze the constant-amplitude data from Reference 6. Effective ranges of stress intensity were calculated from $\Delta K_{eff} = U\Delta S \sqrt{\pi a}$, where the values of a are average crack lengths for the increments of crack growth in Reference 6 and $U = 0.5 + 0.4R$ $(R \geq 0)$, Reference 7. A least-squares technique using the relation $\frac{\Delta a}{\Delta N} = C[\Delta K_{eff}]^n$ produced a good correlation between crack-growth rate and ΔK-effective as shown in Figure 3 for tests at room temperature and 560 K, respectively. The best-fit constants determined for the two test temperatures are given in the following tabulation.

Test temperature	C	n
Room temperature	5.5×10^{-8}	3.15
560 K	1.1×10^{-7}	2.72

These values were used to make the following calculations of crack growth for the variable-amplitude tests.

Variable-Amplitude Tests

Crack-growth rates for the present variable-amplitude tests were calculated in three ways:

(1) By assuming one cycle per flight, and using effective stress intensity.

(2) By considering only the stresses exceeding the crack-opening level, and using effective stress intensity (the "crack-closure method").

(3) By considering all stresses in the flight, and using the conventional stress intensity, ΔK (the "linear-summation method").

Factors to account for the narrow specimen width and the eccentricity of the individual cracks at the two ends of the notch (see Fig. 4) were used to calculate the stress intensities. The width of the specimen was accounted for by the factor $\sqrt{\sec\left(\frac{\pi a}{W}\right)}$ (Ref. 8) and eccentricity was accounted for by factors L interpolated from the tabular values in Reference 9. Thus, the expression for stress intensity was $UASL\sqrt{\pi a \sec\left(\frac{\pi a}{W}\right)}$, where a is the average crack length for the current growth increment, L is the factor for either the long or the short crack, as appropriate, and $U = 1$ to calculate conventional stress intensity. The stress concentration due to the notch in the specimen was neglected because Reference 10 showed it would influence the stress intensity by less than about 3 percent for the present calculations.

For all three methods of calculating crack growth, the stresses selected were from flights of the severity shown in Figure 2 because they represented about 80 percent of the flights applied. All three calculations also assumed

that cracks would grow at the rates determined in constant-amplitude tests for the same values of stress intensity.

One Cycle per Flight—This calculation assumed that a single cycle between the minimum and maximum stresses in the flight (the ground-air-ground cycle) produced all the crack growth. Both type-A and type-C tests were analyzed in this way using effective stress intensity. The "R" value for the ground-air-ground cycle is -0.37. The effective stress range for constant-amplitude tests with negative R values, was determined by elasto-plastic, finite-element analysis of a cracked sheet in Reference 11. Those calculations produce U = 0.54 for the present tests (R = -0.37). For this first method, crack-growth rates (growth increments per flight) were calculated from $\Delta a = C(\Delta K_{eff})^n$ using C and n from the previous section, and using the average crack length from each increment of the experimental crack growth, in ΔK_{eff}. Experimental rates were assumed to be constant during each increment of crack growth.

Crack Closure—For this method, effective stress intensities were calculated for all stress cycles exceeding the crack-opening stress. Only the stress cycles in climb exceed the crack-opening stress when U = 0.54; the cycles in cruise are only partially above (and were neglected), and the cycles for descent are below the crack-opening stress. Therefore, the effective stress range selected was from the maximum stress of each cycle to, arbitrarily, the minimum stress for the smallest amplitude of the climb segment. As Figure 2(a) shows, the climb segment of type-A flights had 30 cycles of small amplitude, 6 cycles of an intermediate amplitude, and 1 cycle of large amplitude. Thus, for this method, crack growth per flight was calculated from

$$\Delta a = C\,[30(\Delta K_{eff})_1^n + 6(\Delta K_{eff})_2^n + (\Delta K_{eff})_3^n],$$

where the subscripts correspond to the three ranges of the effective stress, and the other nomenclature is the same as previously described.

The values of C and n used in the calculations depended on the kind of test. For accelerated tests, the calculations used the values of C and n corresponding to the constant test temperature. For real-time tests, each flight included a temperature cycle, but the temperature for the climb segment of each flight was near room temperature; therefore, values of C and n for room temperature were used.

Linear Summation—This calculation summed the crack growth for the complete range of each cycle in the flight, including the ground-air-ground cycle. Crack growth was calculated using ΔK. To calculate crack growth using ΔK, a different value of "C" was required for each different stress range in the flight. The "C's" were obtained by factoring the term U from the expression for ΔK_{eff}, and combining U with the value of C determined earlier in this paper for constant-amplitude data. Thus, $\frac{\Delta a}{\Delta N} = CU^n(\Delta K)^n = \bar{C}(\Delta K)^n$. The values of $\bar{C}$ obtained using $U = 0.5 + 0.4R$ (Ref. 7) and the constant-amplitude data from Reference 6 are shown in Figure 5. A value of $\bar{C}$ was determined for each stress range in the flight. The previously determined values of the exponent n were retained. The crack-growth rates per flight were calculated from

$$\Delta a = 30\bar{C}_1(\Delta K_1)^n + 6\bar{C}_2(\Delta K_2)^n + \ldots .$$

where the subscripts on $\bar{C}$ and ΔK correspond to the various stress amplitudes, the number of terms in the equation corresponds to the number of

different amplitudes, and the coefficient of each term is the number of cycles for each amplitude.

RESULTS AND DISCUSSION

The test results, presented in Table 1, are discussed in terms of both crack initiation and crack growth.

Crack-Initiation Periods

The smallest cracks detectable from the film records of room-temperature accelerated tests, or from observations of the real-time tests, were usually less than 1 mm long; but the cracks were about 2 mm long before becoming detectable on film records of accelerated tests at 560 K.

In most tests, cracks at the two ends of the notch initiated at different times. Therefore, in general, an eccentricity factor was required to calculate stress intensity for these cracks, as described earlier. The values given in Table 1 for accelerated tests are for the first crack to initiate. For real-time tests, the values are for the first crack at the notch having the median life.

To establish a consistent base of comparison, the number of flights to produce a crack 1 mm long (see Table 1) was determined from plotted curves of crack length versus number of flights for each test. For hot accelerated tests, the curves were extrapolated. Table 1 indicates that most of the cracks reached a length of 1 mm ("initiated") at between 60 and 80 percent of the total life. In all of the accelerated tests, the crack initiation periods were consistently larger fractions of total lives for lower design mean stresses. The data for real-time tests show the opposite trend, but its significance cannot be adequately determined because data are available for only two real-time tests.

Crack-Growth Periods

The periods of crack-growth in Table 1 are differences between the fatigue lives and the initiation periods. The crack-growth periods for type-A accelerated tests at the two temperatures were about the same, consistent with the crack-growth periods for constant-amplitude tests of this alloy from Reference 6 for the same temperatures. For a given design stress, the growth periods for real-time tests were somewhat shorter than for the accelerated tests.

The growth periods for type-A tests were much shorter (growth rates were faster) than for type-G tests. The faster rates for type-A tests indicate that the small stress cycles contributed significantly to the crack growth.

Crack-Growth Rates

The calculated crack-growth rates are plotted against the experimental rates from the present tests in Figures 6 and 7. The points in each figure represent the rates for both the long and short cracks and for all design stresses. The solid line in each figure is a least-squares linear fit of all the points. The dashed lines indicate where the points would lie if the calculated rates equaled the experimental rates.

Type-G Tests—Figure 6 shows the crack-growth rates for type-G tests where both the tests and calculations simulated the flights by a single cycle. As shown by the slope of the solid line, the calculated rates were faster than the experimental rates by an average of about 70 percent. That result should be expected qualitatively, because the higher stresses in fifth flights, 100th flights, and so forth, probably retarded the crack growth, and these higher stresses were not accounted for in the calculations.

Type-A Tests—The experimental crack-growth rates for type-A tests and the rates calculated in the three ways discussed earlier are shown in Figure 7. Parts (a), (b), and (c) of Figure 7 contain the rates for accelerated tests at room temperature, accelerated tests at 560 K, and real-time tests, respectively. The top parts of Figures 7(a), 7(b), and 7(c) compare the experimental rates to those calculated assuming the flight could be represented analytically as a single cycle; the center parts compare the experimental rates to those calculated accounting for only the cycles exceeding the assumed crack-opening level (all the cycles in the climb segment of each flight); the bottom parts compare the experimental rates to those calculated using linear summation of the crack-growth contributions of all cycles in the flight.

Figure 7 shows better agreement between calculated and experimental rates for room-temperature accelerated tests (Fig. 7(a)) than for elevated temperature or real-time tests (Figs. 7(b) and 7 (c)). It shows that the flights were poorly represented in the calculations by a single cycle (top row of figures). It shows that the rates calculated by the crack-closure and the linear summation methods were about equal for each test condition (center and bottom figures).

The present calculations using linear summation and conventional linear fatigue damage calculations both predicted longer fatigue lives (slower damage accumulation) than the experiments produced (see Ref. 5). In contrast, References 1 and 2 reported that linear summation calculations for crack growth indicate higher crack-growth rates than their experiments on 2024-T3 and 7075-T6 aluminum alloys. These different observations probably result from the interaction effects of the spectrums on the materials, the relative severities

of the spectrums, or the combined effects. As shown in Figure 8, the spectrum from Reference 1 contains significantly higher stresses than the present spectrum, relative to the yield strengths of the two materials. Conceivably, the higher relative stresses in the infrequent flights of Reference 1 produced larger delays in crack growth than in the present tests.

In contrast to the good agreement between calculated and experimental rates for the room-temperature tests, the calculated crack-growth rates for accelerated tests at 560 K and for real-time tests were much slower than the experimental rates. This discrepancy is difficult to explain for the hot accelerated tests because the calculation method was identical to that for room-temperature tests, and the supporting constant-amplitude data for both temperatures seemed equally well correlated. Possibly the high loads in the infrequent flights produced less retardation at 560 K than at room temperature. For the real-time tests, Figure 7(c), insufficient information is available about local high-stress creep, stress-strain relations, crack-opening stresses, and their interactions during cycles of temperature, to properly predict crack growth. A first attempt to calculate local stresses at the notch for real-time flights (Ref. 12) indicated only slight differences between the stresses for real-time flights and those for room-temperature flights. Thus, much basic study will probably be required before crack growth can be calculated accurately for this type of loading.

Overall, the present calculations indicate that the linear summation and crack-closure concepts produced the best calculations of crack growth. The calculations by both methods could probably be improved by considering a crack-growth relation which allows the rate to accelerate at high values of stress intensity (see Ref. 13), and by considering the plasticity and

stress distribution effects induced by the notch (see Ref. 14). In addition, calculations with the crack-closure concept could probably be improved through further study of the crack-opening stress levels for variable temperature and loading.

Scanning-Electron Fractographs

Fractographs of specimens from one constant-amplitude test, one type-G test, one type-A accelerated test at each temperature, and one real-time test were prepared and studied for their contribution to understanding crack growth (see Figs. 9-13, respectively). The direction of crack growth is indicated by an arrow for all parts of each figure. Part (a) of Figures 9-13 shows the fracture surface from one end of the central notch toward the edge of the specimen.

Study of the fractographs at moderate and high magnifications indicates very distorted features, such as multiple-plane cracking, secondary cracking, irregular crack fronts, and irregular crack growth, in all tests. Figure 9 shows the fracture surface of a specimen tested under constant-amplitude loading (Ref. 5) with $R = -0.29$ and a maximum stress of 480 MPa. That test condition corresponds approximately to the present GAG cycle in a 10,000th flight with a design mean stress of 241 MPa. In that constant-amplitude test, multiple cracks initiated from the notch and along the fracture surface; (arrows A in Figure 9(b) identify many planes of cracking at the edge of the notch). The planes were joined by shear steps in the fracture surface; see, for example, arrows B in Figure 9(b), and numerous other locations identifiable as white marks parallel to the direction of crack growth in Figures 9(a)-9(e). The planes of crack growth sometimes overlapped. In one instance the

overlapping planes and associated shear steps produced the loose "chip" shown within the arrows in Figure 9(e).

Relatively little area contained easily identifiable markings. The regions C on Figure 9(c) show more markings than is typical of the overall fracture surface. These visible marks are in recessed areas and were apparently protected during the repeated compressive load cycles. Other locations such as D have a smashed appearance which indicates they were not protected during compressive loading.

Figure 9(f) shows the dimple features typical of the static fracture, which is easily distinguishable from the fatigue fracture.

Figure 10, for a specimen from a type-G variable-amplitude test, also shows evidence of multiple-plane crack growth. The variable-amplitude loads produced characteristic bands, some of which are marked by arrows A and B, Figure 10(a). Combinations of large loads and long cracks producing almost critical conditions, caused the large crack advance in mixed mode shown at B in Figure 10(a). The final failure, at C in Figure 10(a), produced the dimple appearance shown at higher magnification at the bottom of Figure 10(b). Although not shown, the region between the shear lips at B is also dimpled. Figure 10(b) shows that the crack front at failure was very irregular as indicated by the dashed line. The irregular features of the fatigue part of the fractograph suggest that the crack front was similarly irregular throughout the growth of the crack. Combinations of secondary cracking and shear steps evident at arrow D suggest a crack-growth mechanism like that which produced the chip in Figure 9 for constant-amplitude loading.

Figure 11(a), for a specimen from a room-temperature flight-by-flight test, shows many bands due to the severe flights. Most of the bands can be

seen without magnification. Figures 11(b) to 11(e) show the irregular shape of the growing fatigue crack by the waviness of the features, like those shown in Figure 10(b). Regular fatigue marks exist only in narrow protected "recesses" such as shown in Figures 11(c) and 11(e). The recesses are not representative of the overall fractograph but they are the only regions containing fatigue markings which suggest both the individual flights and the cycles within the flights.

The fractograph for a specimen from a type-A test at 560 K, Figure 12, shows fewer visible bands than at room temperature. In fact, the only bands identifiable were made by the two most severe flights (a 10,000th flight and a 1000th flight). The multiple-plane cracks and irregular shapes discussed earlier are evident here also, but the texture as shown in Figure 12(c) has a more "brittle" appearance than for the previous room-temperature tests. By careful study of Figure 12(c) using the known sequence of flights and cycles within them, the crack growth during the 1000th flight was associated with the region shown. The bright band between the arrows in Figure 12(c) marks the end of the band visible on the specimen. That visible mark (bright band) is probably made by the negative half of the largest cycle in the flight. The remainder of the flight produced the remainder of the region marked in Figure 12(c). Similarly, Figures 10 and 11, for room-temperature tests indicated that the visible mark is within the band of crack growth caused by the flight.

Figure 13, for the real-time test, shows the visible bands due to the severe flights, but no fatigue detail was detectable at high magnifications. The fracture has a staticlike appearance all over. The reason for the lack of fatigue detail is unknown.

In summary, all of the variable-amplitude tests produced visible marks on the fracture surfaces of the specimens. But the irregular crack growth, and lack of fatigue detail, suggest that attempts to correlate crack-growth rate with these available markings would be pointless. The difficulties in "reading" these fractographs where the stress sequence was known exactly suggest that little detailed information about crack growth could be obtained from failure-analysis fractography for supersonic transport airplane loadings and environments with unknown loading sequences. Whether these complicated fractographic features resulted from the variable-amplitude loading, the compressive loading of the GAG cycle, the material, or some combination of these considerations would probably be a fruitful area for further study.

CONCLUDING REMARKS

Crack growth in Ti-8Al-1Mo-1V was measured and calculated for real-time and accelerated simulations of supersonic airplane loading and heating. Crack-growth rates calculated on the assumption that an entire flight could be represented by a single cycle predicted the experimental rates poorly. Calculated crack-growth rates were slower than the experimental rates for all tests with flight-by-flight loading. For room-temperature accelerated tests, the calculated rates agreed well with the experimental rates; but the calculations became progressively less accurate for progressively more complex test conditions (tests that included elevated temperature). Calculations of crack growth using the crack-closure concept can probably be improved through study of crack-opening stresses using finite-element models that account for variable-amplitude loading, residual stresses, and temperature effects. The calculations of crack growth could also be improved through detailed studies of material properties

and interactions among stress, temperature, and time as appropriate for the real-time operating conditions of a supersonic transport airplane.

Little quantitative information about crack growth was available from scanning-electron fractographs because little fatigue detail was present.

REFERENCES

[1] Schijve, J., Jacobs, F. A., and Tromp, P. J., "Fatigue Crack Growth in Aluminum Alloy Sheet Material Under Flight Simulation Loading. Effects of Design Stress Level and Loading Frequency," NLR-TR-72018U, National Aerospace Laboratory, Amsterdam, Feb. 1972.

[2] Brussat, T. R., "Approach to Predicting the Growth to Failure of Fatigue Cracks Subjected to Arbitrary Uniaxial Cyclic Loading," Damage Tolerance in Aircraft Structures, ASTM STP 486, American Society for Testing and Materials, 1971, pp. 122-143.

[3] Anon., "Metallic Materials and Elements for Aerospace Vehicle Structures," Department of Defense, MIL-HDBK-5A, 1966.

[4] Imig, L. A., and Illg, Walter, "Fatigue of Notched Ti-8Al-1Mo-1V Titanium Alloy at Room Temperature and 550 F (560 K) With Flight-by-Flight Loading Representative of a Supersonic Transport," NASA TN D-5294, National Aeronautics and Space Administration, 1969.

[5] Imig, L. A., and Garrett, L. E., "Fatigue-Test Acceleration With Flight-by-Flight Loading and Heating to Simulate Supersonic-Transport Operation," NASA TN D-7780, National Aeronautics and Space Administration, 1973.

[6] Hudson, C. Michael, "Studies of Fatigue Crack Growth in Alloys Suitable for Elevated Temperature Applications," NASA TN D-2743, National Aeronautics and Space Administration, 1965.

[7] Elber, Wolf, "The Significance of Fatigue Crack Closure," Damage Tolerance in Aircraft Structures, ASTM STP 486, American Society for Testing and Materials, 1971, pp. 230-242.

[8] Brown, William F., and Srawley, John E., "Plane Strain Crack Toughness Testing of High Strength Metallic Materials," ASTM STP 410, American Society for Testing and Materials, 1966, p. 78.

[9] Isida, M., "Crack Tip Stress Intensity Factors for the Tension of an Eccentrically Cracked Strip," Dept. of Mech. Lehigh Univ., Bethlehem, Pennsylvania, 1965.

[10] Newman, J. C., Jr., "An Improved Method of Collocation for the Stress Analysis of Cracked Plates With Various Shaped Boundaries," NASA TN D-6376, National Aeronautics and Space Administration, 1971.

[11] Newman, J. C., Jr., "A Finite-Element Analysis of Fatigue Crack Closure," Presented at the Eighth ASTM National Symposium on Fracture Mechanics, Providence, Rhode Island, Aug. 1974.

[12] Boeing Aerospace Co., "Cyclic-Stress Analysis of Notches for Supersonic Transport Conditions," NASA CR-132387, National Aeronautics and Space Administration, 1974.

[13] Forman, R. G., Kearney, V. E., and Engle, R. M., "Numerical Analysis of Crack Propagation in Cyclic Loaded Structures," Transactions, American Society of Mechanical Engineers, Ser. D, J. Basic Eng., Vol. 89, No. 3, Sept. 1967, pp. 459-464.

[14] Crews, John H., Jr., and White, N. H., "Fatigue Crack Growth From a Circular Hole With and Without High Prior Loading," NASA TN D-6899, National Aeronautics and Space Administration, 1972.

TABLE 1—TEST PROGRAM AND RESULTS
Duplex-annealed Ti-8Al-1Mo-1V, 1.27 mm thick

Stress sequence	Design mean stress, MPa	Fatigue life, flights	Crack initiation[a]		Crack growth[b]	
			Period, flights	Percentage of total life, flights	Period, flights	Percentage of total life, flights
Accelerated tests at room temperature[c]						
A	172	137,158	127,000	93	10,160	7
	207	18,540	13,300	72	5,240	28
	241	7,472	5,300	71	2,170	29
G	172	105,988	78,000	74	27,990	26
	207	57,290	40,300	70	16,990	30
	241	22,290	12,000	54	10,290	46
Accelerated tests at 560 K[c]						
A	172	36,243	25,500	70	10,740	30
	207	12,498	------	--	------	--
	241	4,580	2,850	62	1,730	38
Real-time tests[d]						
A	172	19,014	12,000	63	7,010	37
	207	10,420	8,100	78	2,320	22
	241	5,093	------	--	------	--

[a]For cracks extending 1 mm from the notch.

[b]For cracks from 1 mm long until failure.

[c]One test at each design stress.

[d]Median value from test.

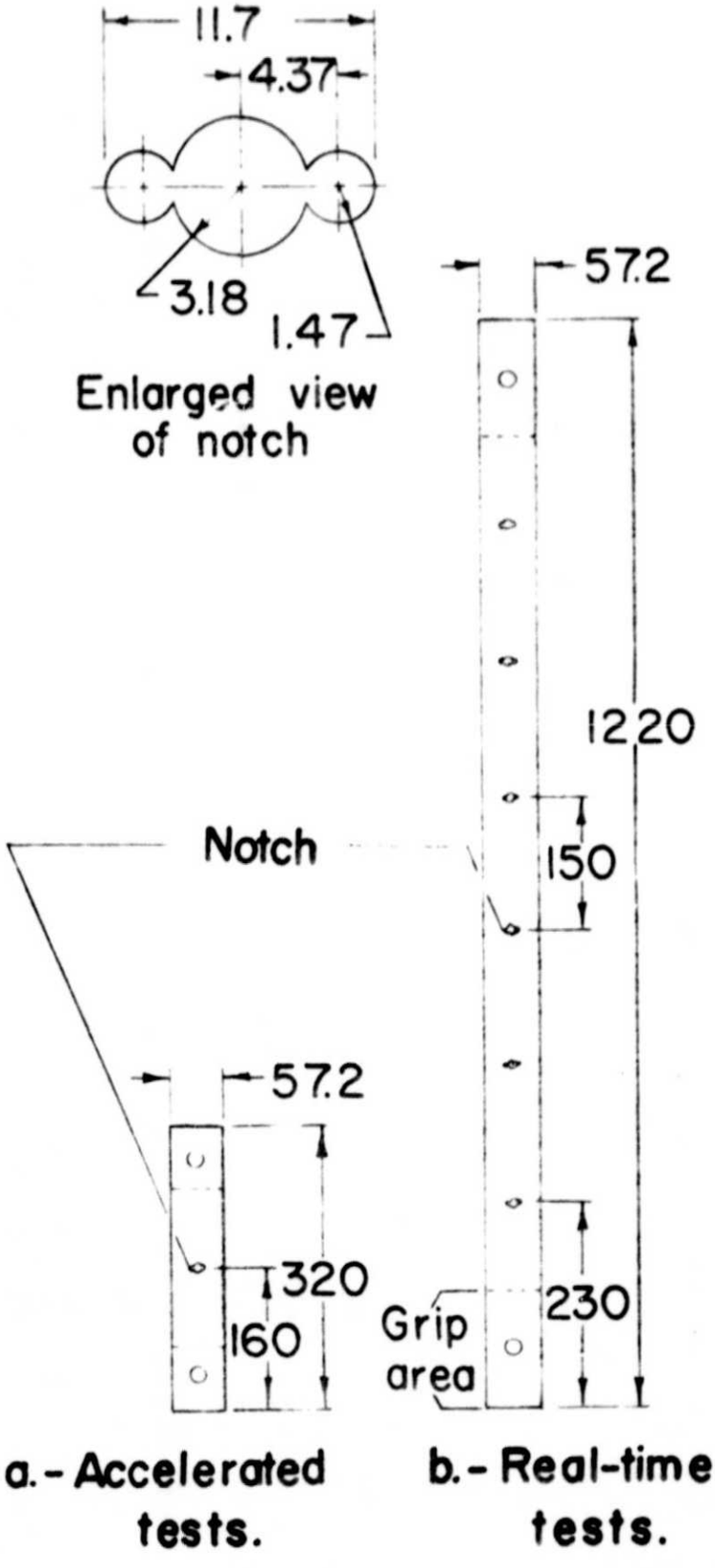

Figure 1. Configurations of fatigue specimens. Dimensions are in millimeters. Sheet thickness is 1.27

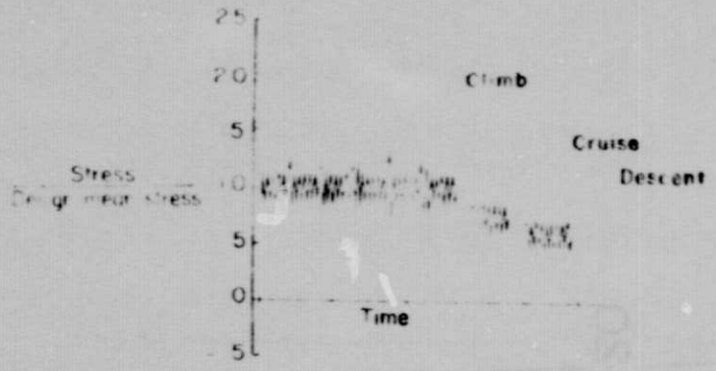

(a) A type A flight for accelerated tests

(b) A type-G flight for accelerated tests

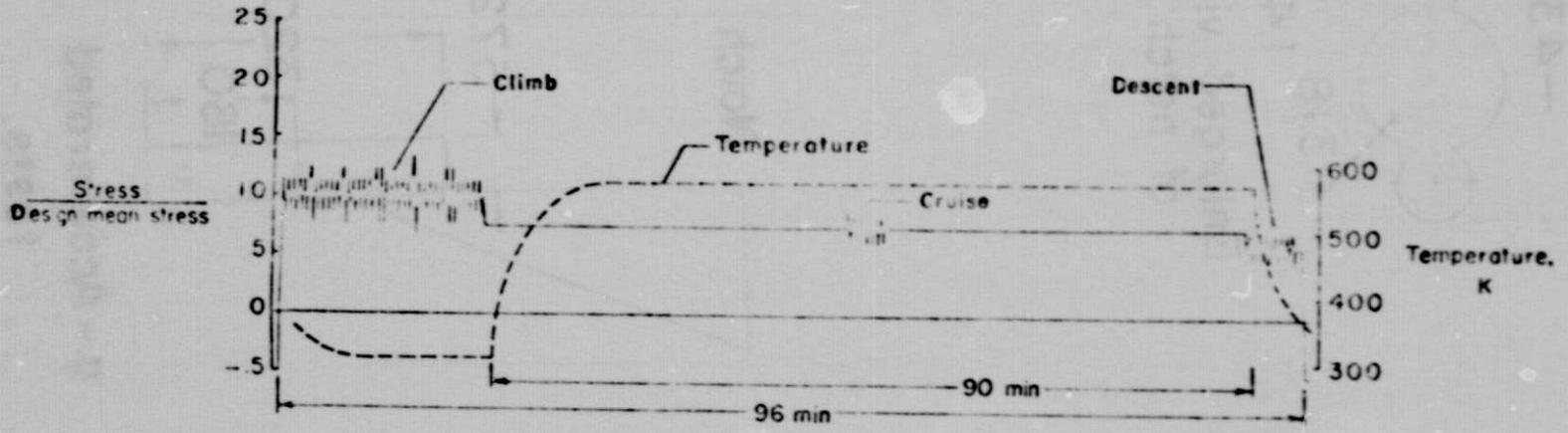

(c) A type-A flight with cyclic temperature for real-time tests

Figure 2. Flights for accelerated and real-time tests.

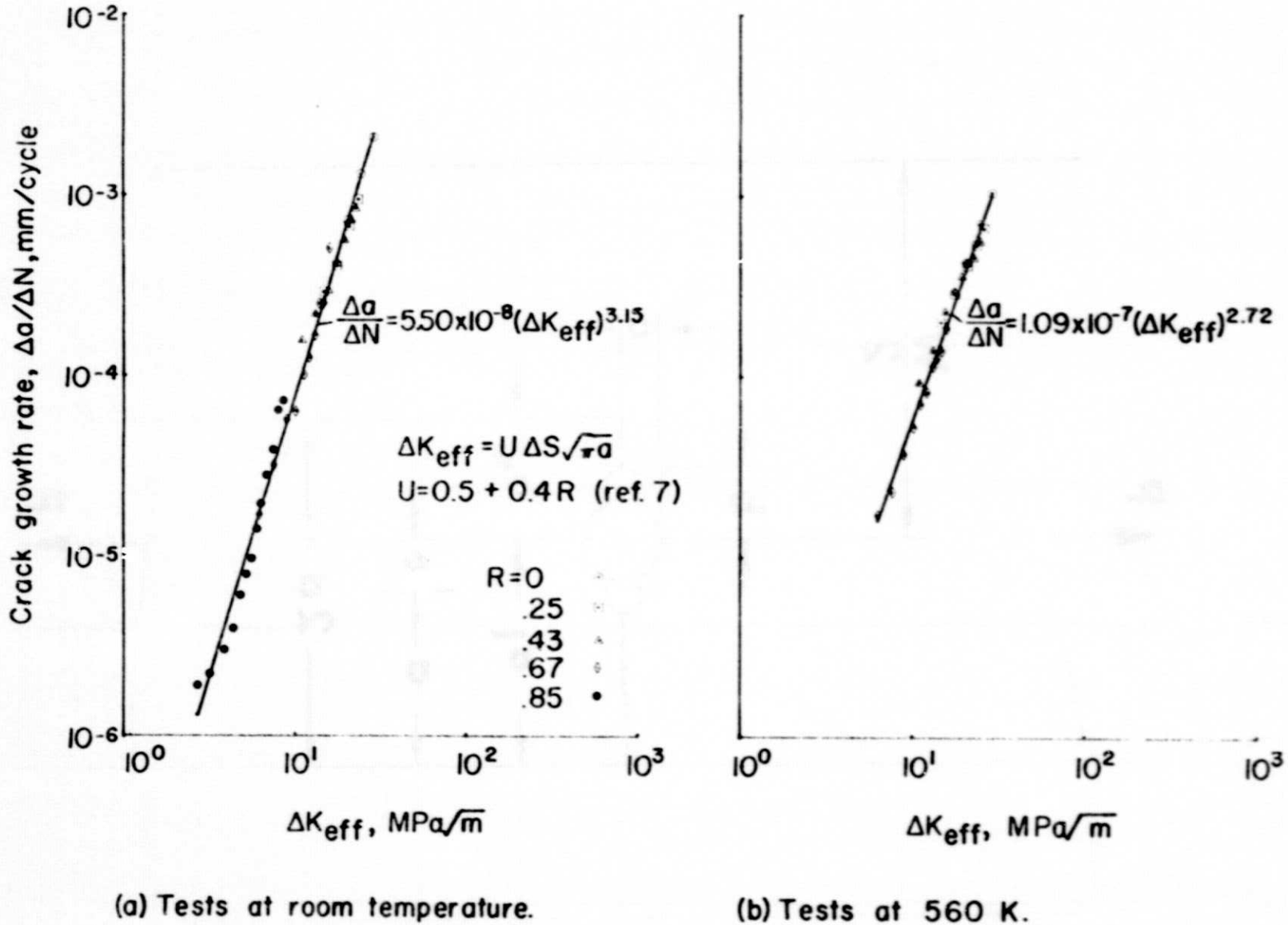

(a) Tests at room temperature.

(b) Tests at 560 K.

Figure 3. Correlation between crack-growth rate and ΔK_{eff} for constant-amplitude fatigue tests of duplex-annealed Ti-8Al-1Mo-1V, 1.27 mm thick. Data from Reference 6.

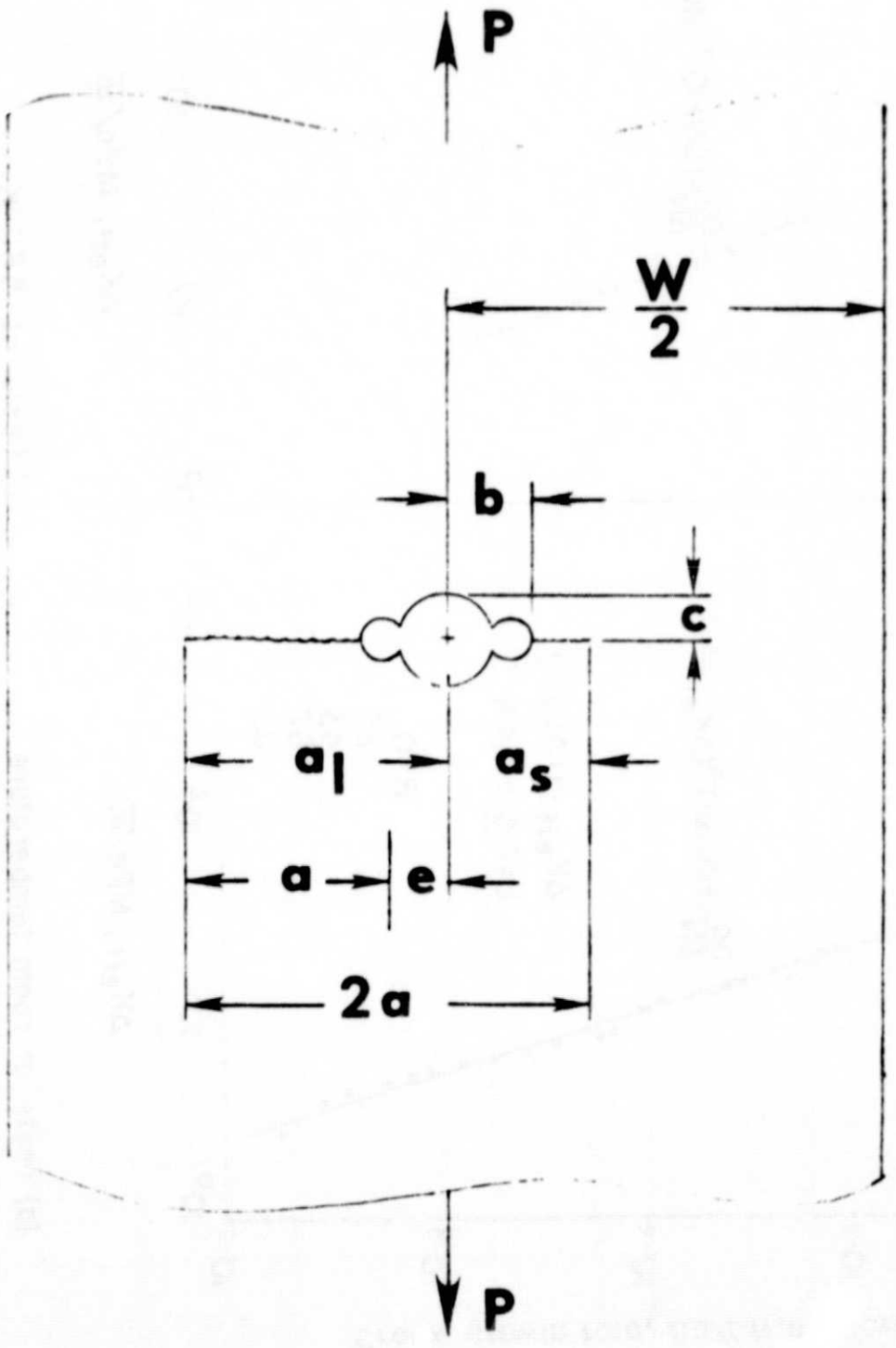

Figure 4. Crack and geometric nomenclatures for calculating crack eccentricities.

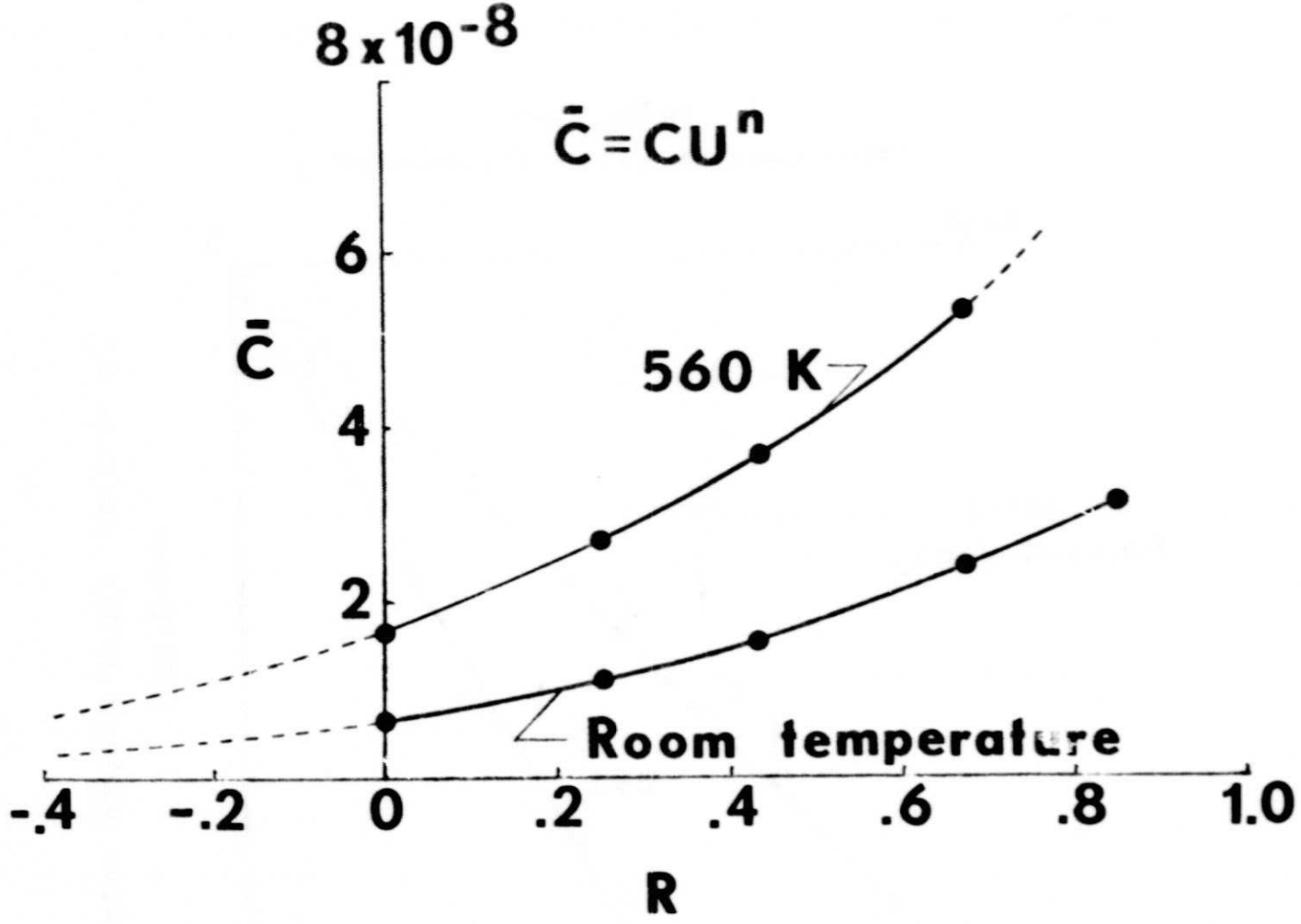

Figure 5. Relations between $\bar{C}$ and R for constant-amplitude fatigue tests of duplex-annealed Ti-8Al-1Mo-1V, 1.27 mm thick. Data from Reference 6.

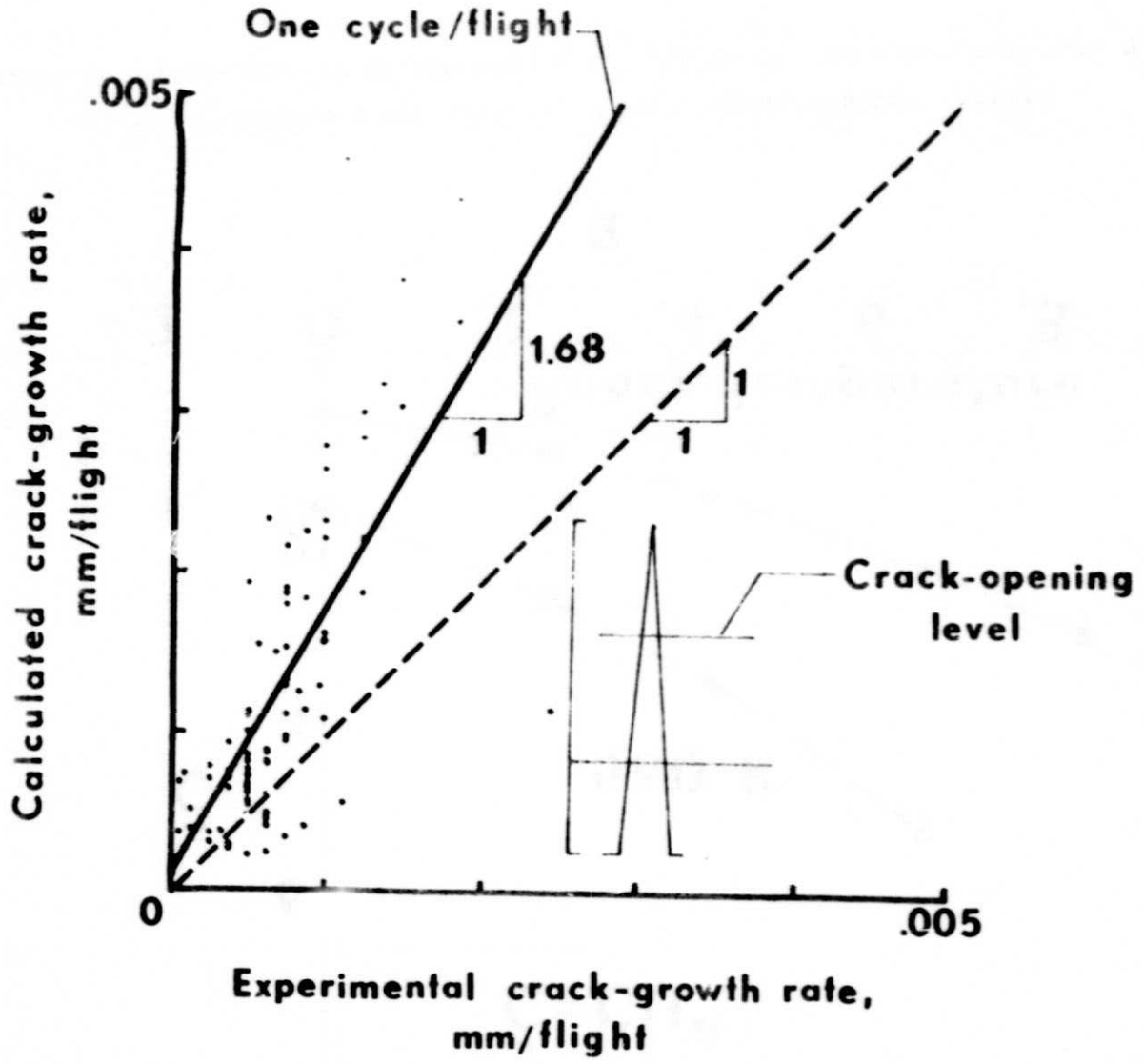

Figure 6. Experimental and calculated crack-growth rates for type-G fatigue tests of duplex-annealed Ti-8Al-1Mo-1V, 1.27 mm thick.

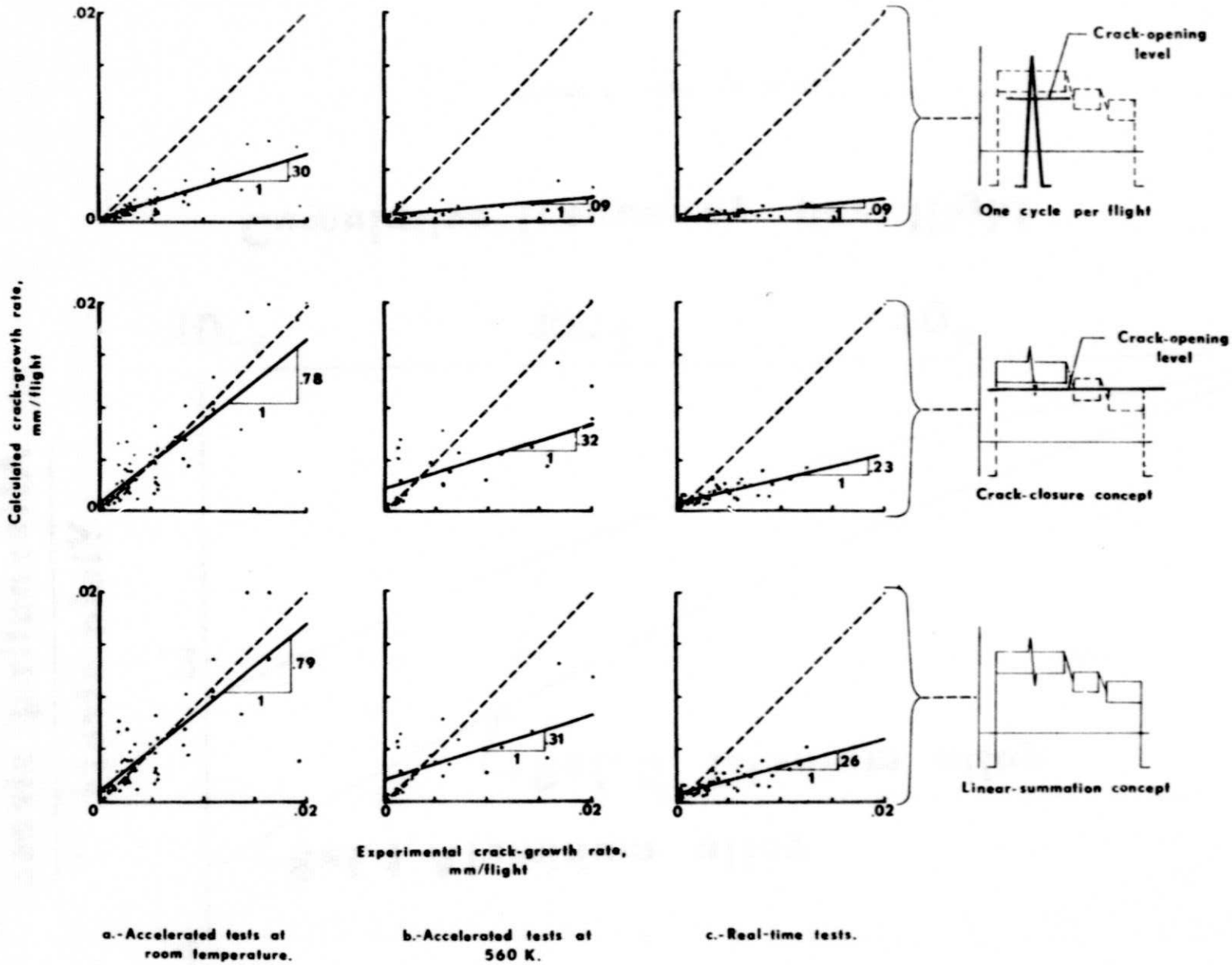

Figure 7. Experimental and calculated crack-growth rates for type-A fatigue tests of duplex-annealed Ti-8Al-1Mo-1V, 1.27 mm thick.

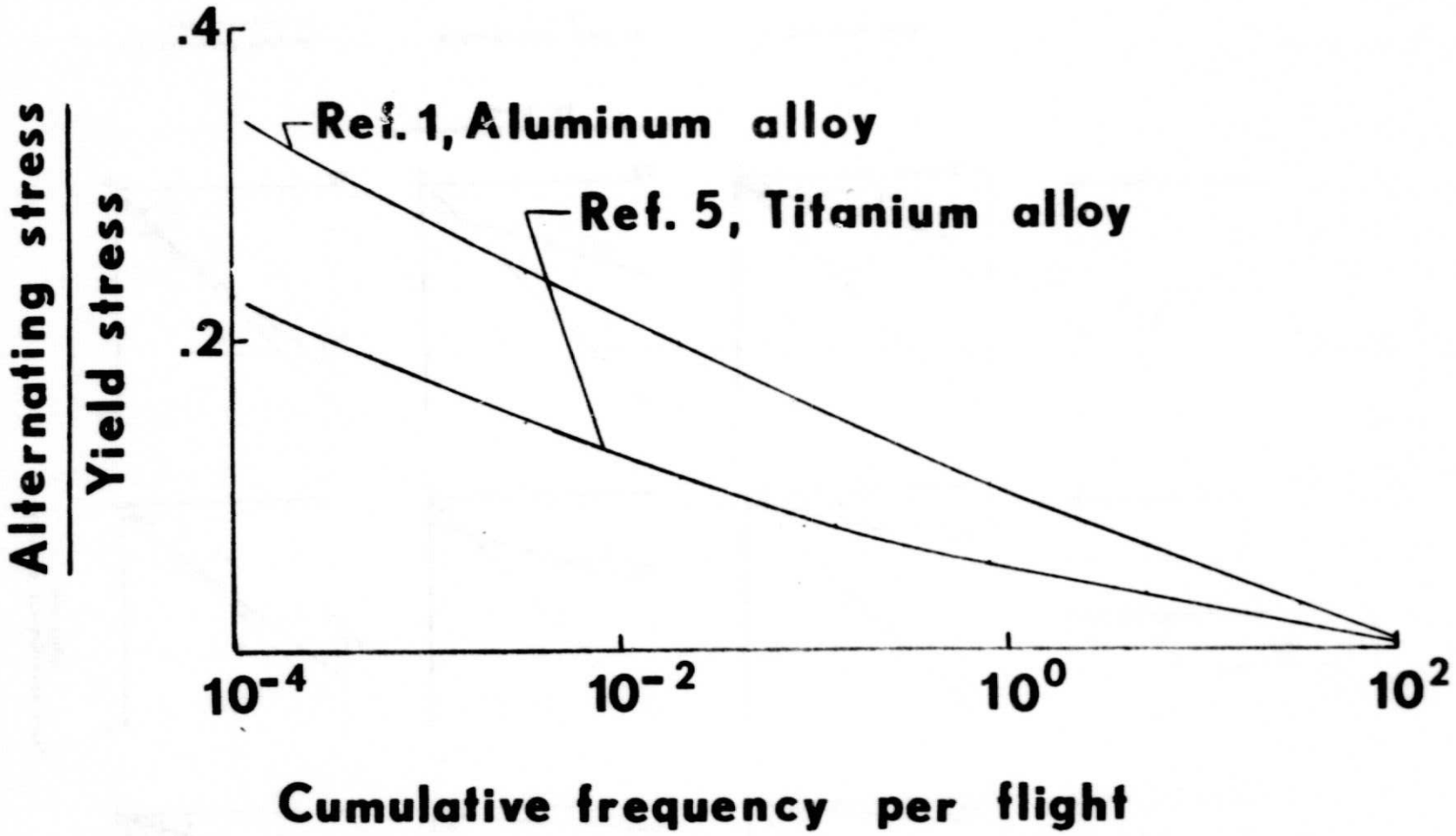

Figure 8. Gust spectrums.

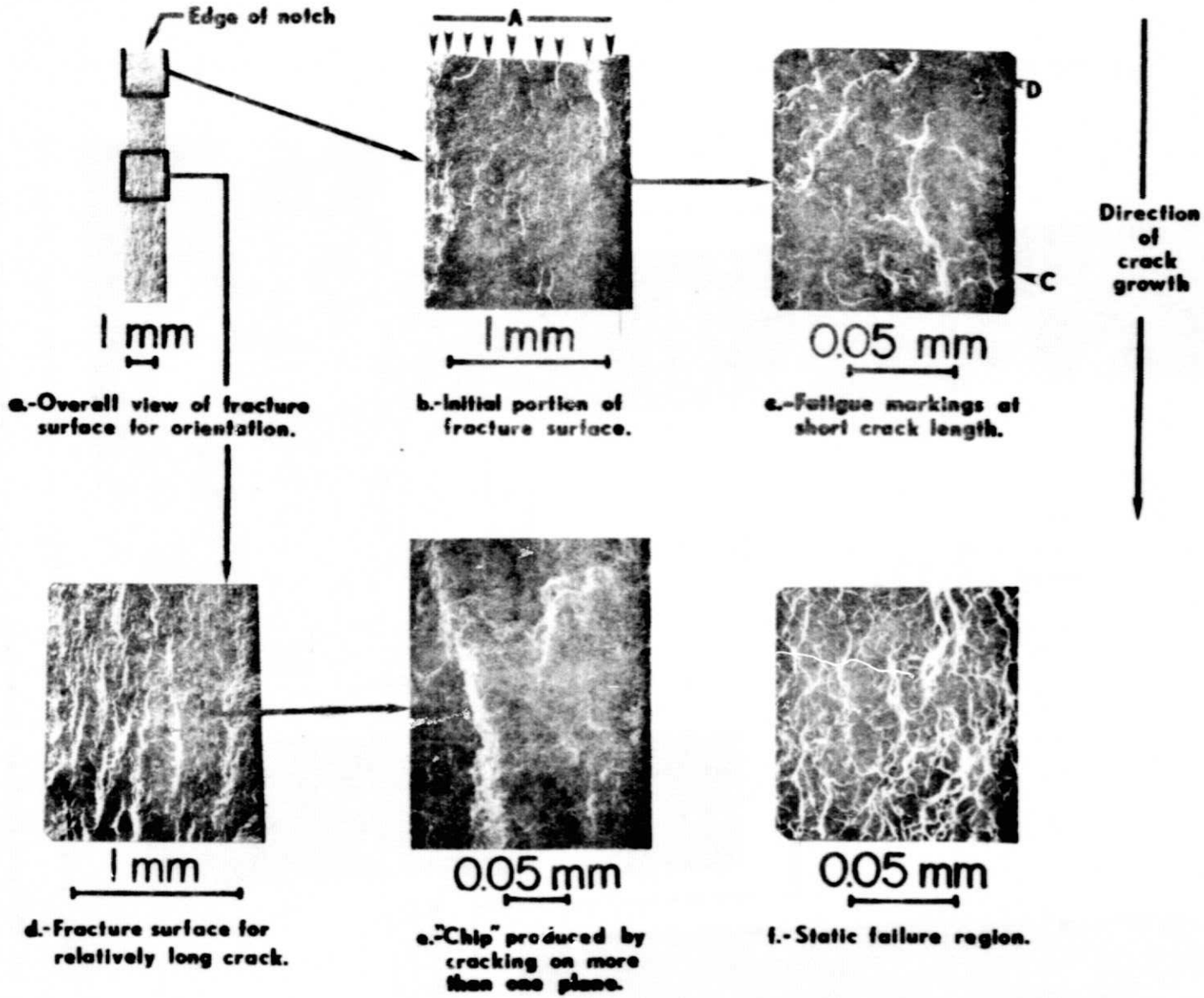

Figure 9. Scanning-electron fractographs of a specimen from a constant-amplitude fatigue test at 560 K (from Ref. 5). Duplex-annealed Ti-8Al-1Mo-1V, 1.27 mm thick. Maximum stress = 480 MPa, R = -0.29.

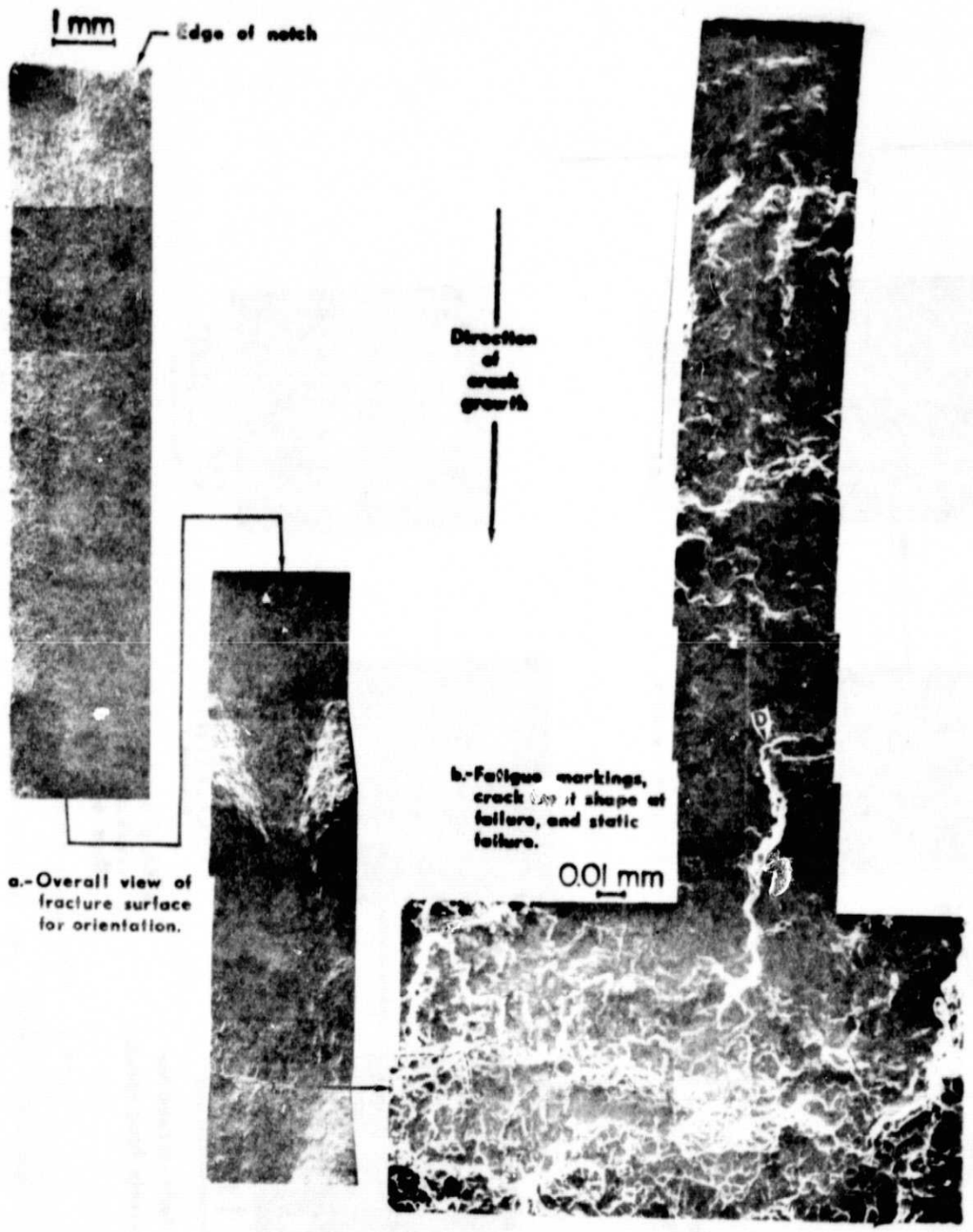

Figure 10. Scanning-electron fractographs of a specimen from an accelerated type-G fatigue test at room temperature. Duplex-annealed Ti-8Al-1Mo-1V, 1.27 mm thick. Design stress = 241 MPa.

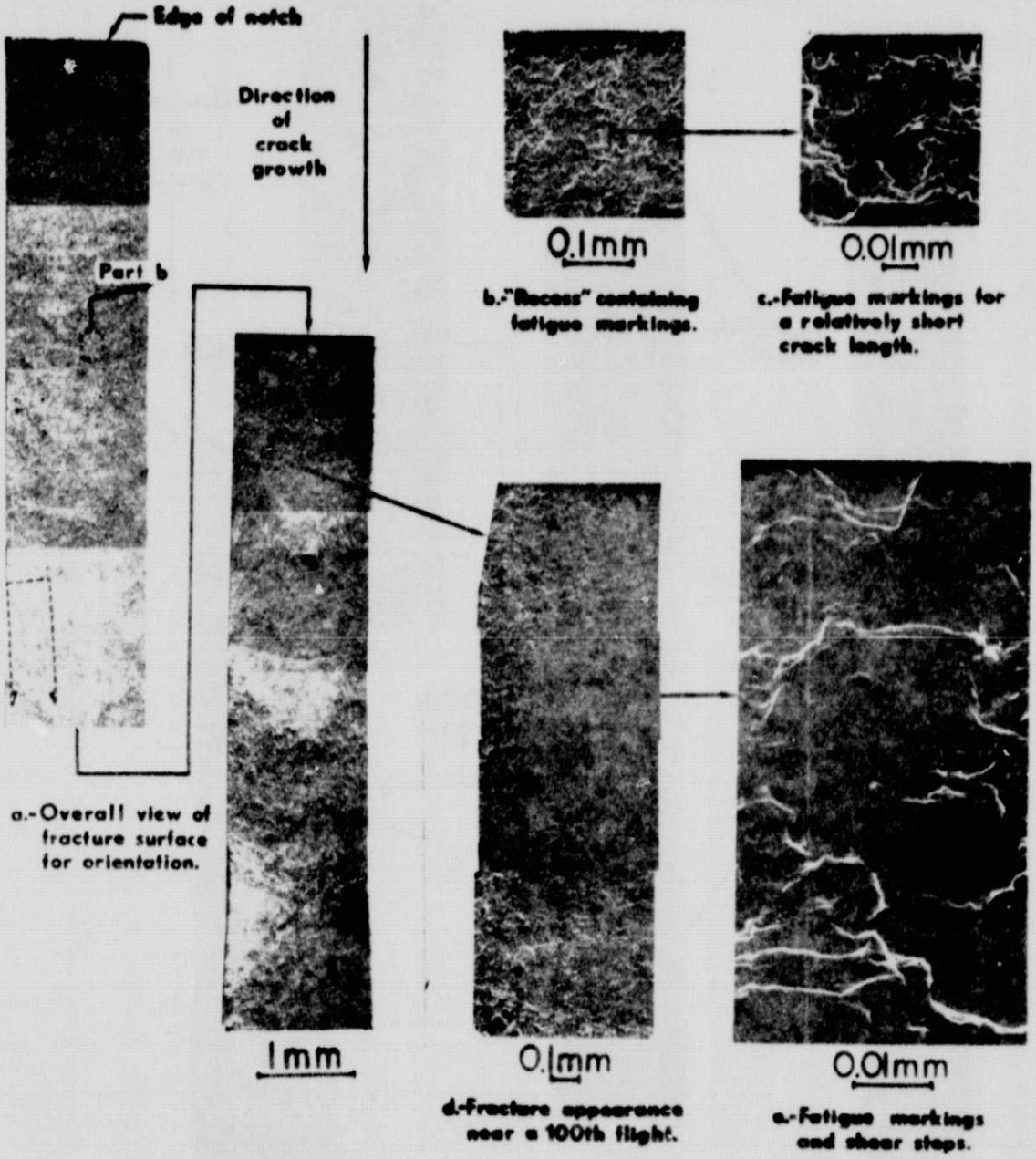

Figure 11. Scanning-electron fractographs of a specimen from an accelerated type-A flight-by-flight fatigue test at room temperature. Duplex-annealed Ti-8Al-1Mo-1V, 1.27 mm thick. Design stress = 241 MPa.

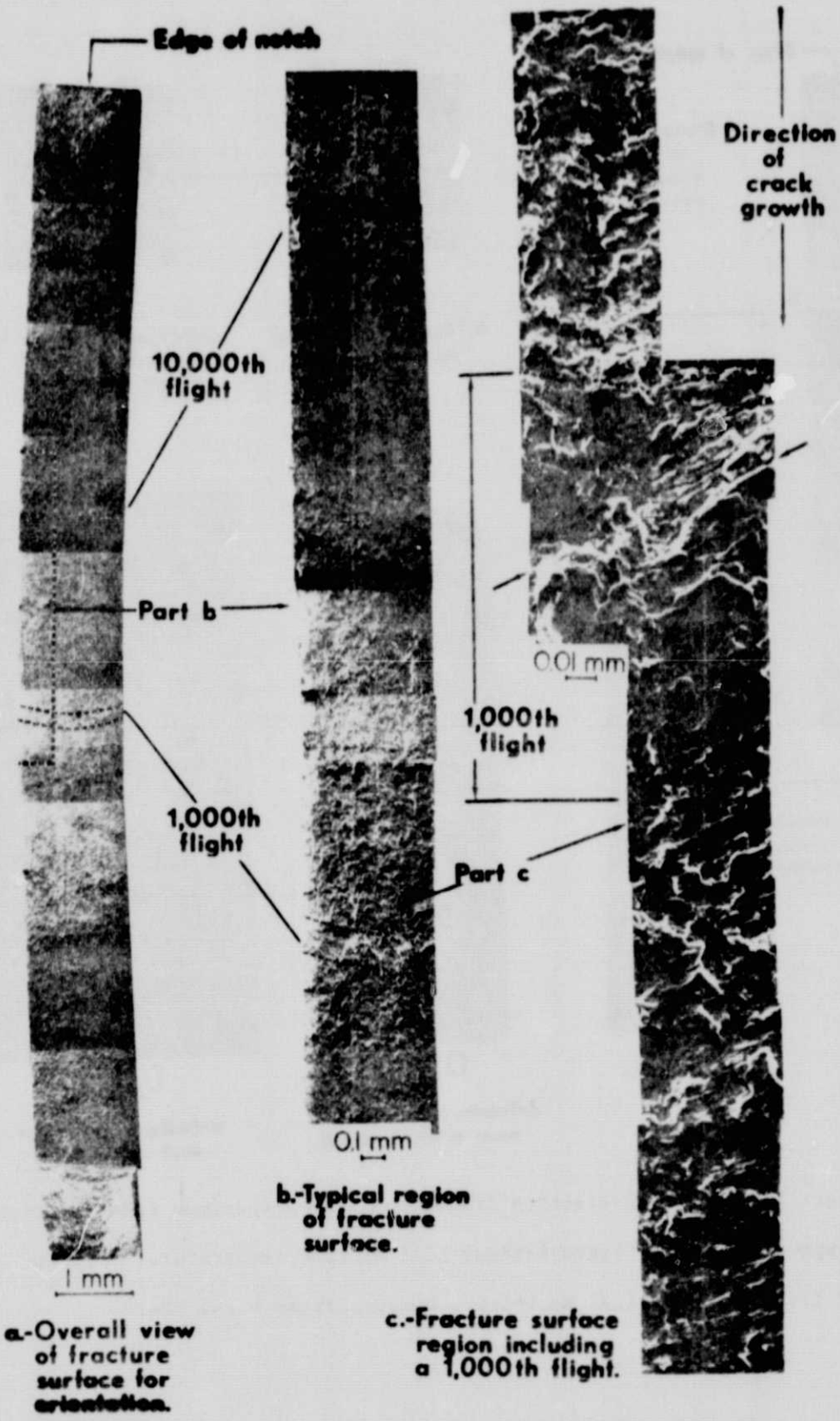

Figure 12. Scanning-electron fractographs of a specimen from an accelerated type-A flight-by-flight fatigue test at 560 K. Duplex-annealed Ti-8Al-1Mo-1V, 1.27 mm thick. Design stress = 207 MPa.

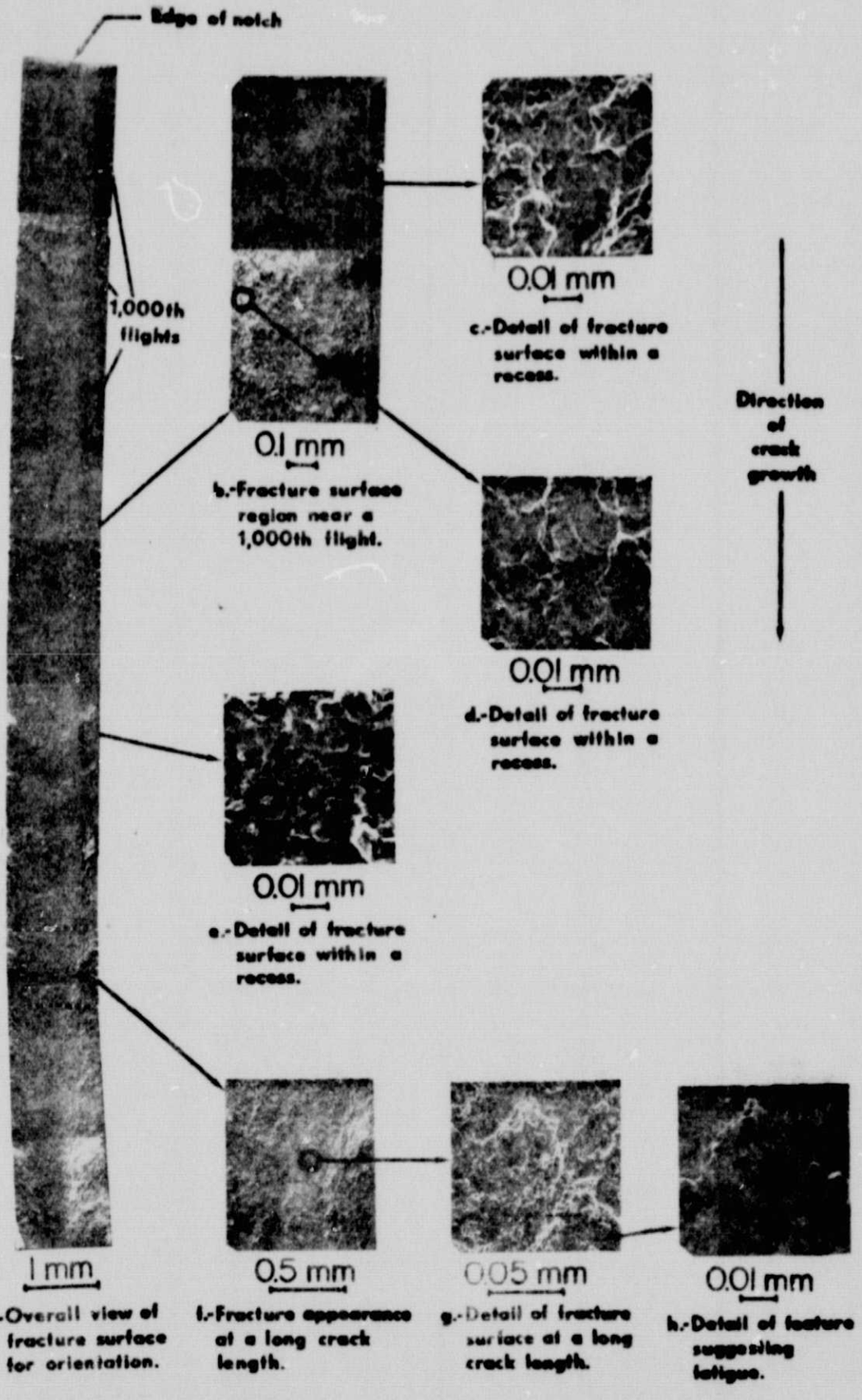

Figure 13. Scanning-electron fractographs of a specimen from a real-time type-A flight-by-flight fatigue test. Duplex-annealed Ti-8Al-1Mo-1V, 1.27 mm thick. Design stress = 207 MPa.